

# Study of viscous oil-water-gas slug flow in horizontal pipes

P. Babakhani Dehkordi <sup>a\*</sup>, L.P.M. Colombo <sup>b</sup>, E.Mohammadian <sup>c,d\*</sup>, D. Arnone <sup>e</sup>,  
A.Azdarpour <sup>f</sup>, G. Sotgia <sup>b</sup>

**a:** Politecnico di Milano, Department of Energy, via Lambruschini 4, 20156 Milan, Italy

**b:** Politecnico di Milano, Department of Energy, via Lambruschini 4, 20156 Milan, Italy

**c:** Department for Management of Science and Technology Development, Ton Duc  
Thang University, Ho Chi Minh City, Vietnam

**d:** Faculty of Applied Sciences, Ton Duc Thang University, Ho Chi Minh City, Vietnam

**e:** VGV srl, Calvisano (BS), Italy

**f:** Department of Petroleum Engineering, Marvdasht Branch, Islamic Azad University,  
Marvdasht, Iran

**Corresponding author\*:** Parham Babakhani Dehkordi ([Babakhani65@gmail.com](mailto:Babakhani65@gmail.com))

**Co-corresponding author\*:** Erfan Mohammadian ([erfan.mohammadian@tdtu.edu.vn](mailto:erfan.mohammadian@tdtu.edu.vn))

## 1. Introduction

Understanding liquid-liquid-gas flow is crucially important for production and transportation systems. There have been numerous investigations regarding two-phase flows in the past few years. However, a few research works have been performed, even using low viscosity oil, in three phase flows. As an example of three phase flows, the work by Acikgoz et al. (1992) can be cited, which deals with the identification of low viscosity oil/water and gas flow patterns within a horizontal pipe with an ID=19 mm. They used low oil viscosity ( $\mu_o=0.116$  Pa·s at

24 25 °C) and density of  $864 \text{ kg}\cdot\text{m}^{-3}$ . The investigated operating conditions were as  
25 follows: superficial water velocity ( $J_w=0.66 \text{ m}\cdot\text{s}^{-1}$ ), superficial oil velocity ( $J_o=0.24$   
26  $\text{m}\cdot\text{s}^{-1}$ ), and superficial gas velocity (extended to  $50 \text{ m}\cdot\text{s}^{-1}$ ). Many different flow  
27 patterns were recognized depending upon the fact that water and oil maintain their  
28 structures as continuous flow, defined as water-based and oil-based flow,  
29 respectively. Several attempts were made to utilize conductance sensors for  
30 measuring phase holdup and automatizing flow pattern recognition in two-phase  
31 flow, as suggested by Gao et al. (2016, 2017, 2018), but universal tools and  
32 methods are not yet available, particularly for three-phase flows.

33 Series of research activities have been conducted at the test facilities (WASP) at  
34 Imperial College, London. The work by Pan et al. (1995) deals with oil/water/gas  
35 flow within an ID=76.2 mm and ID=38.0 m long horizontal pipes. Experimental  
36 tests were performed at 0.5 MPa test facilities and operating conditions was similar  
37 to Acikgoz et al. (1992). Hewitt (2005) conducted liquid-liquid-gas flow tests with  
38  $\mu_o= 0.04 \text{ Pa}\cdot\text{s}$  and high flash point oil. The pressure drop and liquid phase holdups  
39 using dual-energy gamma densitometer were measured. Two different behaviors  
40 were observed from the analysis of pressure drop measurements depending on gas  
41 flow rates. A peak at pressure drop was observed confirming the presence of  
42 inversion mechanism for higher gas flow rate. Accordingly, water continuous flow  
43 converts to oil-based continuous flow and effective viscosity becomes so high that  
44 it considerably increases pressure drop, see also the works by Hall (1992) and  
45 Odozi (2000). On the other hand, at low gas velocity, the peak of pressure drop was  
46 not observed. Keskin et al. (2007) suggested a two-step categorizing technique.

47 Twelve individual flow patterns were identified in a horizontal pipe, considering  
48 very low oil viscosity. Malinowsky (1975) carried out slug flow tests with  $\mu_o=4-5$   
49 mPa.s, ID=38.1 mm as well as operating pressure of 2 bar. Superficial gas, water,  
50 oil velocities were ranged, respectively, within the intervals as follows:  $1.5 < J_g < 4.3$   
51  $\text{m}\cdot\text{s}^{-1}$ ,  $0.19 < J_w < 2.08 \text{ m}\cdot\text{s}^{-1}$ , and  $0.26 < J_o < 1.36 \text{ m}\cdot\text{s}^{-1}$ . The major observed flow pattern  
52 under investigation was slug flow, with a few tests corresponding to high gas flow  
53 rates, in which misty annular and slug was observed. He compared pressure drop of  
54 his experimental data with classical correlation of Beggs and Brill (1973), which is  
55 broadly applicable in oil industry, assuming that oil-water mixture had a linear  
56 interpolated viscosity. Finally, he concluded that linear approximation for mixture  
57 viscosity of oil-water is a poor representation due to the fact pressure drop  
58 predictions are up to 50% underpredicted. Stapelberg and Mewes (1994) measured  
59 distributed pressure gradient and slug frequency using a laser, concerning three-  
60 phase flow with  $\mu_o=0.031 \text{ Pa}\cdot\text{s}$  and  $\rho_o=886 \text{ kg}\cdot\text{m}^{-3}$ . The tests were investigated in  
61 two different pipe diameters as 23.8 and 59 mm. Flow patterns were also detected  
62 and flow maps were developed.

63 Issa, et al (2007) studied oil-water-gas flow within a straight duct with ID=77.92  
64 mm. Low oil viscosity ( $\mu_o=45.8 \text{ mPa}\cdot\text{s}$ ) was considered for the tests. They  
65 examined different aspects of slug structures in terms of spatial distribution of each  
66 phase. Time-averaged liquid holdups, slug frequency were measured by using two  
67 X-ray and gamma systems, which were capable of differentiating between water  
68 and oil. It was observed that slug frequency is reduced as a result of increasing  
69 water cut at fixed superficial gas and liquid velocities. Furthermore, a peak of slug

70 frequency at lower water cut was detected, suggesting the inversion mechanism  
71 from oil to water continuous flow.

72 Multiphase flows of high viscous oil/water/gas behave differently from flows of  
73 low viscous oil/water/gas. The main reason arises from the rheological property of  
74 oil phase. In spite of the importance of high viscous oil/water/gas flows in oil  
75 industry, few studies have been conducted in horizontal pipes. The work by  
76 Bannwart (2009) can be cited, considering very viscous oil-air-water flows ( $\mu_o=3.4$   
77 Pa·s,  $\rho_o=970$  kg.m<sup>-3</sup> at T=20 °C) within a 28.4 mm i.d. pipe (Laboratory scale) and a  
78 77 mm i.d. pipe (full-scale facility). The tests were performed both in a horizontal  
79 and upward vertical pipe, the influence of inclination angle on three-phase flow  
80 pattern was investigated. Nine flow patterns were identified in horizontal pipe  
81 which are Bubble gas-Bubble oil ( $B_g, B_o$ ), Bubble gas-Annular oil ( $B_g, A_o$ ), Bubble  
82 gas-Intermittent oil ( $B_g, I_o$ ), Bubble gas-Stratified oil ( $B_g, S_o$ ), Intermittent gas-  
83 Bubble oil ( $I_g, B_o$ ), Intermittent gas-Annular oil ( $I_g, A_o$ ), Intermittent gas-  
84 Intermittent oil ( $I_g, I_o$ ), Stratified gas-Bubble oil ( $S_g, B_o$ ), Stratified gas-Stratified oil  
85 ( $S_g, S_o$ ). Superficial gas, water, and oil velocities varied as follows:  $J_g=0.03-10$  m·s<sup>-1</sup>,  
86  $J_w=0.04-0.5$  m·s<sup>-1</sup>,  $J_o=0.01-2.5$  m·s<sup>-1</sup>. They presented pressure drop data and  
87 concluded that the existence of gas phase has a positive influence on increasing  
88 frictional pressure loss. Pressure drop was perceived to be highly dependent upon  
89 superficial velocity of phases. The pressure drop increase caused by gas injection  
90 can be damped by increase of water, promoting the lubrication mechanism and help  
91 preventing oil from adhering to the internal surface of pipe wall. Wang et al. (2013)  
92 carried out oil-water-gas experiments with much lower oil viscosity ( $\mu_o=0.15-0.57$

93 Pa·s at 37.8-15.6 °C). The internal pipe diameter is 52.5 mm, superficial water and  
94 oil velocities varied from 0.1-1 m·s<sup>-1</sup>, and gas superficial velocity ranged 1-5 m·s<sup>-1</sup>.  
95 Flow patterns were monitored and images captured by means of high-speed video  
96 camera. The experimental pressure gradient was compared to the mechanistic  
97 model developed by Zhang and Sarica (2006), showing unsatisfactory agreement.  
98 Table 1 lists a summary of related studies for oil-water-gas flow in horizontal ducts.  
99 The rheological properties of gas and water are not reported because city tap water  
100 and air are used as test fluids in all cases.

101 Since very few experimental data was presented in the literature, the present study  
102 aims at expanding the data related to pressure drop measurement. Moreover, study  
103 of literature survey reveals that hydrodynamic behavior of high viscous oil-water-  
104 gas flow and slug characteristics in horizontal pipe is not well understood. In the  
105 current work, slug frequency was measured by signal analyses and the results were  
106 compared to the available correlations in the literature for gas-liquid flow.  
107 Geometrical dimensions of slug and bubble, which included slug body length ( $L_s$ )  
108 and bubble length ( $L_f$ ) were measured by optical sensor. Statistical analysis of slug  
109 body length (PDFs) was presented. Based on measurements of slug and bubble  
110 length, a new expression for calculating slug unit length in three phase flow high  
111 viscous oil in horizontal pipe is formulated. Translational bubble velocity is  
112 measured by optical probe and video camera, results of bubble velocity ~~was~~ were  
113 compared to the correlation of Nicklin (1962) which is a drift-flux based  
114 formulation. Section 3 reports the results of experimental analyses.

115

116

117

118

119

120 **Table 1.** Summary of experimental investigations on oil-water-gas flow in horizontal ducts

Author	Pipe I.D. (mm)	$\mu_o$ (mPa·s)	$\rho_o$ (kg·m <sup>-3</sup> )	Velocity range (m·s <sup>-1</sup> )
Malinowsky (1975)	38.1	4-5	855	J <sub>o</sub> :0.26-1.36 J <sub>w</sub> :0.19-2.08 J <sub>g</sub> :1.5-4.3
Acikgoz et al. (1992)	19	116	864	J <sub>o</sub> :0.26 J <sub>w</sub> :0.66 J <sub>g</sub> : up to 50.0
Hall (1992)	78	40-60	876.2	J <sub>o</sub> :0-0.54 J <sub>w</sub> :0-0.83 J <sub>g</sub> :0.98-4.1
Stapelberg and Mewes (1994)	23.8; 59	31	858	J <sub>o</sub> :0.062-0.244 J <sub>w</sub> :0.16-0.18 J <sub>g</sub> : not reported
Odozi (2000)	78	9.3-153	855-871	J <sub>o</sub> :0.1, 0.5, 0.7 J <sub>w</sub> :0.05-0.5 J <sub>g</sub> :2.0-24.0
Hewitt (2005)	38; 78	40	860	J <sub>o</sub> : 0.06-0.39 J <sub>w</sub> : 0.21-0.54 J <sub>g</sub> =1.6-11.7
Keskin et al. (2007)	51	13.5	858.8	J <sub>o</sub> :0.02-1.5 J <sub>w</sub> :0.01-1.0 J <sub>g</sub> =0.1-7.0
Issa, et al (2007)	78	45.8	863	J <sub>o</sub> : 0.13-0.37 J <sub>w</sub> : 0.13-0.35 J <sub>g</sub> =3.9-4.4
Bannwart (2009)	28.4; 77	3400	970	J <sub>o</sub> : 0.01-2.5 J <sub>w</sub> : 0.04-0.5

121

122

## 123 2. Experiments

### 124 2.1 Experimental facility and operating procedure

125 The liquid-liquid-gas test rig is located in the Laboratory of Multiphase Thermal-  
126 Fluid Dynamics at Politecnico di Milano. The facility is sketched in Fig. 1 The  
127 rheological properties of fluids are: tap water ( $\mu_w=1.026\times 10^{-3}$  Pa·s,  $\rho_w=999$  kg·m<sup>3</sup>),  
128 Oil (type Milpar 220,  $\mu_o=0.838$  Pa·s,  $\rho_o=890$  kg·m<sup>3</sup>, and  $\sigma_o=0.02$  N·m<sup>-1</sup> at T=20 °C),  
129 air ( $\mu_a=1.98\times 10^{-5}$  Pa·s,  $\rho_a=1.2$  kg·m<sup>3</sup>). The test section is composed of a 12 m long  
130 straight transparent duct with ID=40 mm. The pressure drop measurement was  
131 performed, considering five pressure taps. Each pressure was connected to a  
132 pressure transducer (differential type with full scale: 1 psi = 6.89 kPa), positioned 6  
133 m from pipe inlet. Two K-type thermocouples (10 % Cr-6 % Al) are used to  
134 measure both the ambient and mixture temperature, one is located outside the pipe  
135 and the second one is positioned at almost half distance of the total pipe length.  
136 Variation of volumetric fluxes for oil, water, and air are as follows:  $J_o=0.36-0.71$   
137 m·s<sup>-1</sup>,  $J_w=0.44-1.32$  m·s<sup>-1</sup>, and  $J_g=0.22-2.10$  m·s<sup>-1</sup>. Water and oil flow rates were  
138 measured by using a magnetic flow meter (accuracy  $\pm 0.5\%$  of reading) and a  
139 calibrated gear metering pump, respectively. Oil and water are injected in the pipe  
140 through a coaxial injector in order to aid the onset of formation of core-annular flow

141 in the appropriate range of superficial velocities. Water is drawn first to the test  
 142 section, oil is then supplied with the selected flow rate. Water flow rate is checked  
 143 and its value is adjusted to the set point, if needed. Once the two-phase flow is  
 144 properly formed, the distributed pressure drop is measured. At the final stage, air is  
 145 then introduced at the desired flow rate, and once the three-phase flow is suitably  
 146 stabilized, the distributed pressure drop is measured. A total number of 235 pressure  
 147 drop data points were acquired. The facility is equipped with an optical probe  
 148 developed and designed by Arnone (2017) (see section 2.3) and a video camera (see  
 149 section 2.4 for image processing), positioned 7 and 7.5 m from the inlet, to  
 150 investigate both quantitative and qualitative aspects of three-phase flow.

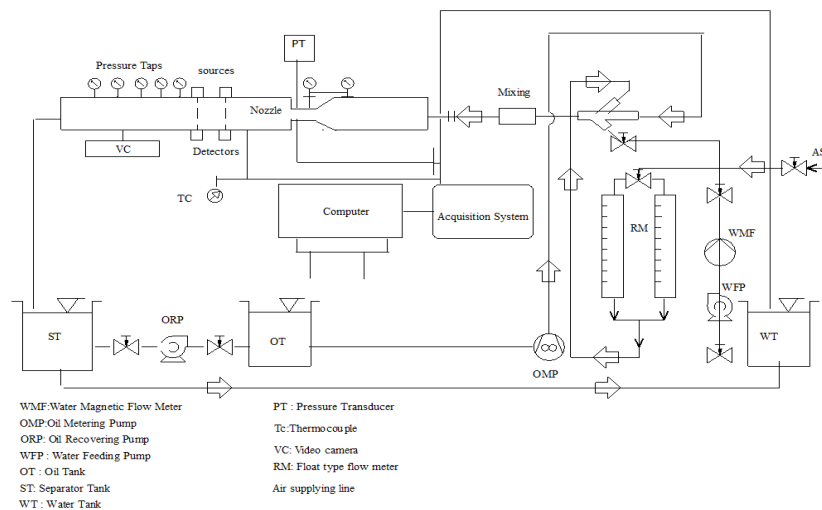


**Fig 1. Experimental setup**

## 2.2 Governing parameters

155 The main controlling parameters are reported in this section. Volumetric flux or  
 156 superficial velocity  $J$  ( $\text{m}\cdot\text{s}^{-1}$ ) for each phase is determined as the ratio between

157 individual volumetric flow rate and area of pipe cross-section, as the phase flowed  
158 alone. The total mixture volumetric flux is computed by summation of individual  
159 superficial velocity of each phase as:

$$160 \quad J_t = J_o + J_w + J_g \quad (1)$$

161 The same definition can be applied to the total liquid superficial velocity as:

$$162 \quad J_L = J_o + J_w \quad (2)$$

163 The ratio between gas/oil/water and total liquid volumetric fluxes is defined as:

$$164 \quad \varepsilon_{Lg} = \frac{J_g}{J_L} \quad \varepsilon_{Lo} = \frac{J_o}{J_L} \quad \varepsilon_{Lw} = \frac{J_w}{J_L} \quad (3)$$

165 The volumetric fraction of a phase is defined as the proportion of superficial and  
166 actual velocity of single phase as follows:

$$167 \quad H_o = \frac{J_o}{U_o} \quad H_w = \frac{J_w}{U_w} \quad H_g = \frac{J_g}{U_g} \quad (4)$$

168 The liquid holdup is then  $H_L = H_o + H_w$ , thus void fraction is  $H_g = 1 - H_L$ .

169 The pressure reduction factor as defined by Bannwart et al. (2004) and Poesio et al.  
170 (2009) is the ratio between liquid-liquid and three phase pressure drop, considering  
171 the same operating conditions for water and oil flow rates, that is;

$$172 \quad R_{LG} = \frac{\Delta p_{oil-water}}{\Delta p_{oil-water-gas}} \quad (5)$$

173 Since flow pattern under investigation is slug flow, and three-phase flow mixtures  
174 are identified by elongated air bubbles, optical techniques, as introduced by Poesio

175 et al. (2009b), have been adopted to determine translational bubble velocity,  $U_t$ .  
176 They are illustrated in the following sections.

177

178

### 179 **2.3 Optical probe measurements data processing**

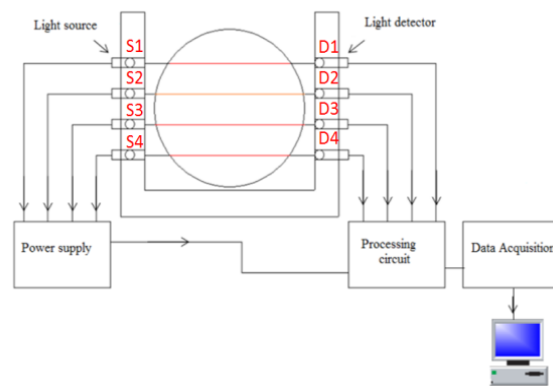
180 In the current study, a non-intrusive optical probe has been designed to measure the  
181 translational velocity of bubbles. During three-phase flows of oil-water-gas,  
182 different configurations of phases can be formed mainly depending on operating  
183 conditions. The phases in contact may have either smooth or wavy interfaces. The  
184 designed optical probe has to be able to detect differences between optical  
185 properties of phases in medium. Moreover, it should be capable of distinguishing  
186 between elongated bubble zone and slug liquid zone. A detailed diagram of the  
187 optical probe is depicted in Fig. 2. It comprises four points LED (Light-Emitting  
188 Diodes, which are positioned such a way that they cover the whole height of the  
189 tube with a spacing of 4 mm), four light-dependent resistance (LDR) detectors and  
190 a processing circuit.

191 LDR sensors are placed at horizontally opposite points to capture the light generated by the  
192 LED source after its passage through the test section. The narrow light beam passes through  
193 the three-phase medium before reaching the LDR, being particularly absorbed, refracted,  
194 reflected, scattered, etc. Hence, intensity of the light captured by the detectors depends on the  
195 spatial distributions of phases. Another optical probe is positioned at an adjustable distance  $L$

196 (30 cm in the present study) in order to generate time-shifted signals, which are used to  
197 determine the bubble translational velocity, as described in the following.

198 Electric output of the probe is obtained at the sampling frequency of 1000 Hz and  
199 saved in a PC for further processing. Because the frequency of slug flow ranged  
200 from 2 to 20 Hz, 1000 Hz is a suitable frequency for detecting it. An example of  
201 raw output signal is shown in Fig. 3 where the black and green signals denote the  
202 uppermost and lowest LEDs, respectively, mounted in a radial direction.

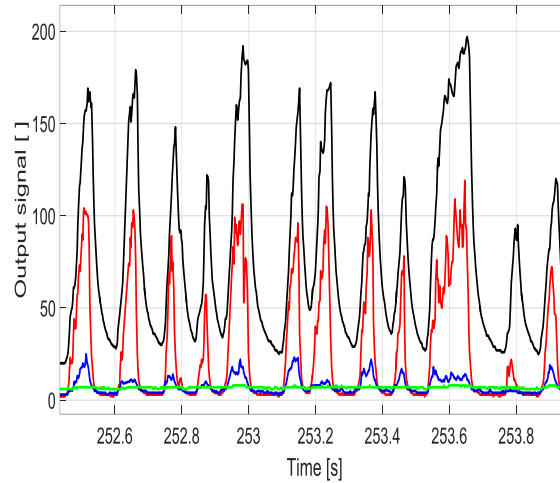
203



204

205

**Fig. 2.** Schematic representation of optical probe device



206

**Fig. 3.** Example of raw output signal for  $J_o=0.71 \text{ m}\cdot\text{s}^{-1}$ ,  $J_w=1.32 \text{ m}\cdot\text{s}^{-1}$ , and  $J_g=2.10 \text{ m}\cdot\text{s}^{-1}$

208 The bubble translational velocity can be detected by knowing the distance (L) between two  
209 probes and associated time lag ( $\tau$ ):

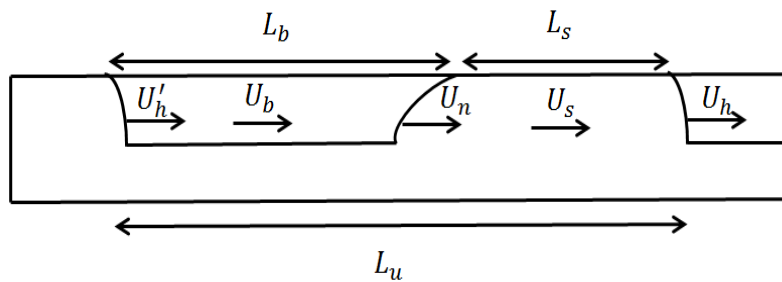
210 
$$U_t = \frac{L}{\tau} \quad (6)$$

211 In all the operating conditions, the intensity of the light captured by the two sensors below the  
212 pipe axis (D3 and D4 in Fig. 2) is very weak, since most of the light path covers the liquid  
213 phase other than gas. On the contrary, the other two sensors (D1 and D2 in Fig. 2) present a  
214 strong response with sharp transitions, marking the passage of air bubbles. Hence, output of  
215 D1 and D2 sensors has been averaged and used for data processing, in order to determine  
216 bubble translational velocity by means of cross-correlation technique. It is worth noting that  
217 distance (L) between two sensible areas (two sensors) needs to be properly selected because it  
218 depends on flow conditions. If bubble are too fast and short, longer distance is required. On  
219 the other hand, if distance is too long, it is difficult to identify the bubble because during the

220 passage of elongated bubbles it may happen that elongated bubbles collide each other and two  
221 sensors see different elements of bubbles. In this case, it is so difficult to obtain a time lag  
222 between two similar signals.

### 223 2.3.1 Single bubble identification method

224 Detection of bubble translational velocity by means of cross-correlation technique is very fast  
225 but it gives only averaged value. Furthermore, structural configurations of slug flow, such as  
226 bubble length cannot be detected. The second approach is based on the so-called “single bubble  
227 identification method”. Fig. 4 shows the schematic representation of slug flow.



228

229 **Fig. 4.** Schematic representation of slug flow

230 As it is evident from Fig. 4, the slug flow pattern is characterized by liquid regions alternating  
231 with elongated air bubbles. Characteristic parameters of slug unit are defined as:

232

233  $U_h$ : velocity of head of leading liquid slug

234  $U_n$ : velocity of tail of leading liquid slug or head of bubble

235  $U'_h$ : velocity of head of trailing liquid slug

236  $L_s$ : liquid slug length

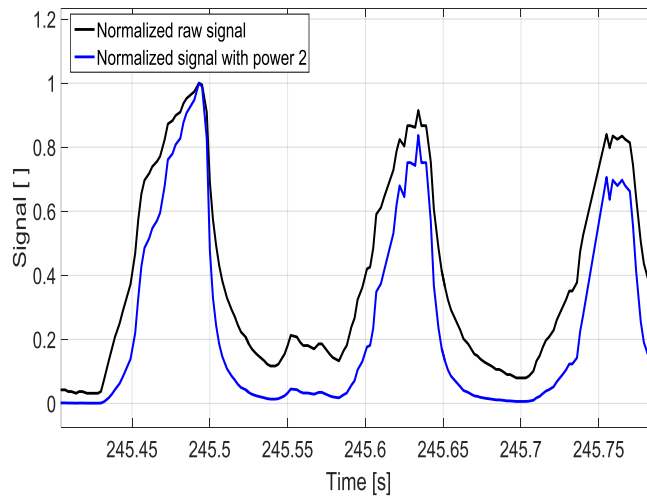
237  $L_b$ : bubble length

238  $L_u$ : total slug unit length

239 The single bubble identification method is an advantageous way to measure the head, tail  
240 velocities of liquid slug and bubble, and geometrical parameter of slug unit. It is worth noting  
241 that velocity of tail of liquid slug,  $U_n$  is equivalent to velocity of head of bubble. First, the raw  
242 signal is normalized with power 2, in order to amplify the difference between bubble and liquid  
243 passage as:

$$244 \quad S = \left( \frac{S - \min(S)}{\max(S) - \min(S)} \right)^2 \quad (7)$$

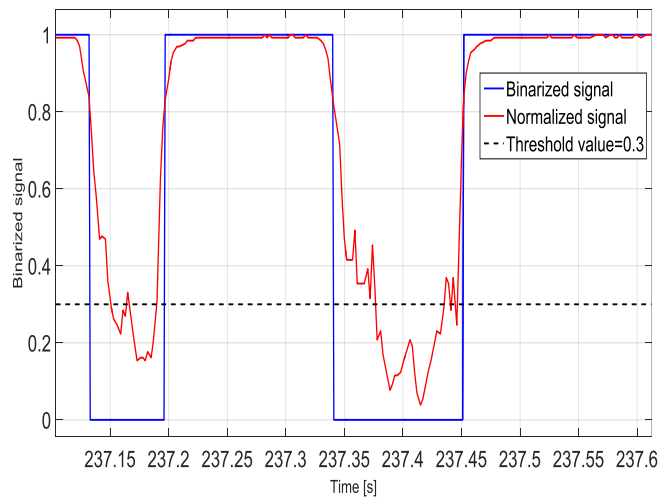
245 An example of signal normalization is illustrated in Fig. 5. After normalization of signal, it is  
246 necessary to convert the normalized signal to a binarized rectangular wave signal, by means of  
247 a threshold value, suitably selected according to the operating conditions to extract some  
248 information about geometrical parameters of slug flow. In the binarized signal, the value 1 and  
249 0 relate to the liquid and gas phase, respectively. Fig. 6 shows typical example of binarization  
250 process with a threshold value set as 0.3, where transition from 0 to 1 indicates the front of a  
251 slug while transition from 1 to 0 indicates the tail of slug. The effect of threshold value on  
252 capturing slug unit must be always checked. The threshold value of 0.3 seems to be a good  
253 approximation because it captures all slug units.



254

255

**Fig. 5.** Example of signal normalization



256

257

**Fig. 6.** Typical example of binarization process using threshold technique

258

259

After detection of rectangular signal, the algorithm is able to extract time residence of slug and

260

bubble. To measure the bubble ( $U_{eb}$ ) and liquid slug velocity ( $U_s$ ), first, the characteristic times

261

of slug unit must be suitably identified. Table 2 shows time residence of slug unit characteristic.

262

**Table 2.** Characteristic time residence of slug unit between two sensible areas

$t_{h2}-t_{h1}$	Time residence of liquid slug head between two sensible area
$t_{n2}-t_{n1}$	Time residence of liquid slug tail between two sensible area
$t_s$	Time passage of liquid slug from first to the second sensor
$t_b$	Time passage of elongated bubble from first to the second sensor

263

264 Since the time residence of head and tail of slug can be detected from binarized signal, the

265 velocity of head and tail of slug is measured by knowing the distance between two sensors as:

266 
$$U_h = \frac{L}{t_{h2}-t_{h1}} \quad (8)$$

267 
$$U_n = \frac{L}{t_{n2}-t_{n1}} \quad (9)$$

268 Slug ( $U_s$ ) and elongated bubble velocities ( $U_{eb}$ ) are measured, simply, by averaging velocity

269 of slug head and tail:

270 
$$U_s = \frac{U_h+U_n}{2} \quad U_{eb} = \frac{U_n+U'_h}{2} \quad (10)$$

271 The bubble and slug lengths would be determined by multiplication of time residence of bubble

272 and slug between two sensible areas and respective velocities.

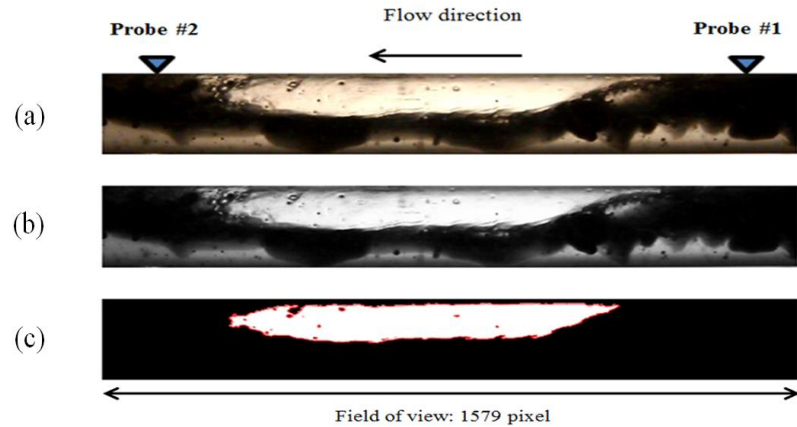
273 
$$L_b = t_b U_{eb} \quad L_s = t_s U_s \quad (11)$$

274 The total slug unit length is the summation of bubble length ( $L_b$ ) and slug body275 length ( $L_s$ ), that is,  $L_u=L_b+L_s$ .276 **2.4 Image processing**

277 The objective of image-processing was to measure translational velocity of slugs.  
278 Other geometrical characteristics of slugs can be directly evaluated from image  
279 processing of video cameras. To extract quantitative information regarding  
280 hydrodynamic behavior of slug flow, a series of images ( $250 \times 1579 \text{ px}^2$ ) were taken  
281 by video camera (NIKON D3300) at frequency 50 fps (frames per second). The  
282 visualization section is exposed by two yellow lamps. One case of the typical flow  
283 pattern is illustrated in Fig. 7. It is seen that oil is mainly opaque, whereas air and  
284 water are transparent. Hence, to distinguish air-oil and water-oil interfaces, a  
285 threshold technique is required. The image post-processing is carried out using  
286 Image Toolbox of Matlab<sup>®</sup>. Bubble translational velocity is computed by means of  
287 cross-correlation, using two virtual probes (probe #1 and 2 in Fig.7), positioned at  
288 the beginning and end of pipe (with known distance  $\Delta x$ ) to ensure that even very  
289 long elongated bubbles can be captured. Therefore, translational velocity is given  
290 by:

$$291 \quad U_t = \frac{|\Delta x|}{N_{frames}} \cdot \text{pixel size} \cdot F_s \quad (12)$$

292 Where  $N_{frames}$  and  $F_s$  (50 fps) are the number of frames passed between two  
293 probes and sampling frequency, respectively.



294

295 **Fig. 7.** Example of image post-processing to detect translational velocity, (a)  
 296 original frame; (b) grey-scale image; (c) binarized frame. The triangles indicate the  
 297 position of virtual probes

### 298 3. Experimental results

#### 299 3.1 Flow pattern

300 Flow patterns were observed by using a digital video camera for viscous oil-water-  
 301 air flow. As the slug flow was the main flow pattern, the classification was made  
 302 based on the interaction between water and oil in liquid slug and film regions.  
 303 Examples of monitored flow patterns are reported in Table 3 where the  
 304 abbreviations are Slug-CA: Slug with oil core/annular water; Slug-FM-PGE: Slug  
 305 with fully mixed oil/water and partial gas entrainment to the slug; Slug-FM-CGE:  
 306 Slug with fully mixed oil/water and complete gas entrainment to the slug. The  
 307 interactions between water and oil in film and slug body regions have not been  
 308 widely known for such complex flow, however, it was investigated that at fixed gas  
 309 velocity the film height for high viscosity flow is much greater (due to lower  
 310 velocity) as compared to the lower viscosity flow (see e.g. Wang et al., 2013 and

311 Shmueli et al., 2015). Additionally, at lower and higher gas velocity, curvy and flat  
 312 gas-liquid interface were observed, respectively (Table 3 a,b). A possible  
 313 explanation for such behavior is because of decreasing the film region height with  
 314 increasing  $J_g$ .

315

316

317

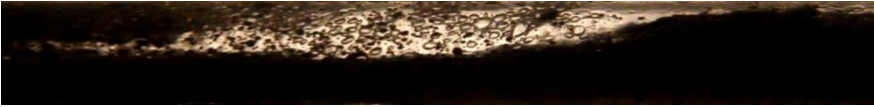
318 **Table 3.** Examples of the monitored flow patterns

319

Direction of flow  
 ←

320

(a)

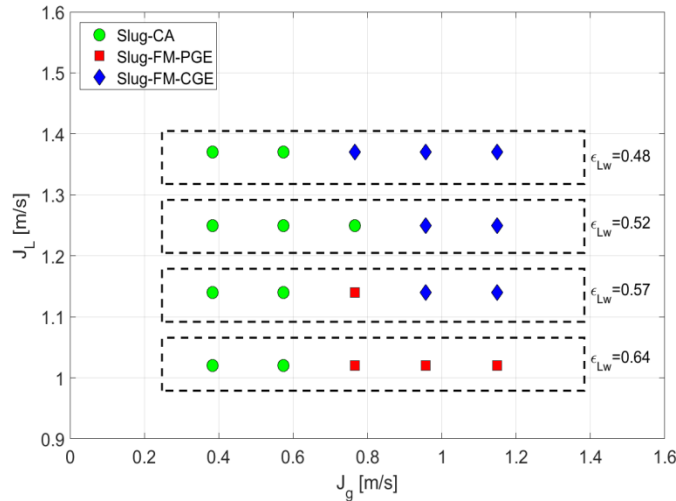
Flow pattern	$J_o$ [ $\text{ms}^{-1}$ ]	$J_w$ [ $\text{ms}^{-1}$ ]	$J_g$ [ $\text{ms}^{-1}$ ]
(b)  Slug with oil core/annular water (Slug-CA)	0.36	0.66	0.57
(c)  Slug with fully mixed oil/water and partial gas entrainment to the slug (Slug-FM-PGE)	0.59	0.88	1.34
	0.77	1.32	1.14

321

322 The results are also shown on flow pattern map where gas and total liquid  
323 volumetric fluxes are considered as abscissa and ordinate, respectively at four  
324 different water cuts:  $\epsilon_{LW}=0.48-0.64$ . At fixed superficial liquid velocity, interaction  
325 between oil and water changes from core-annular flow to fully mixed flow (as  
326 shown itself by the presence of oil drops within water continuous flow) as gas  
327 velocity is increased (see, Fig. 8). Regardless of total superficial liquid velocity, this  
328 transition occurred for  $J_g=0.6-0.8 \text{ m}\cdot\text{s}^{-1}$ . Generally, at lower gas and liquid velocities,  
329 radial components of buoyancy forces overcome (which tend to keep the oil droplet  
330 off-center) drag forces, leading to formation of separated flow regime. Dispersion of  
331 oil into water in the film and slug body regions is highly dependent upon their input  
332 volumetric fluxes.

333 At higher liquid velocities (Table 3, image c), the Taylor bubble front is penetrated  
334 into the leading slug body tail and fragmented to smaller bubbles, as a result, they  
335 are transported and imbibed to the trailing slug body head. This phenomenon is  
336 affected by three main mechanisms, including shear stress caused by a shear layer  
337 between the high-velocity slug head and slow moving of leading liquid film, slug  
338 head vortex (which results from slug head circulation), and gas-carry in the  
339 proceeding liquid film (see Al-safran et al, 2015). The presence of mixing region at  
340 slug body front is not observed by visual inspection (see Table 3, a-c). Therefore, it  
341 is less likely that the second mechanism plays an important role for viscous oil-  
342 water-gas flow. Al-safran et al. (2015) evaluated the influence of high liquid  
343 viscosity on aeration of slug body for oil/gas flow and concluded that viscous forces  
344 overcome turbulent kinetic energy in the slug body mixing region, resulting in

345 reduction of entrainment rate. Although, interaction between the oil-water mixture  
 346 and bubble in the slug head mixing region has still remained obscure for three phase  
 347 flow, it seems from visual observation that the damping effect of viscous oil  
 348 outweighs vortex intensity caused by water (less viscous phase).



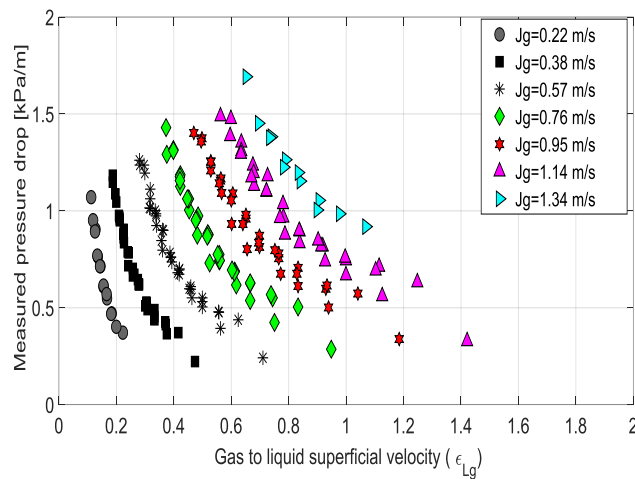
349

350 **Fig. 8.** Oil-water-air experimental flow map for four different Water cuts ( $\epsilon_{Lw}=0.48-0.64$ ). Slug-  
 351 CA: Slug with oil core/annular water flow, Slug-FM-PGE: Slug with fully mixed oil/water flow  
 352 and partial gas entrainment to the slug, Slug-FM-CGE: Slug with fully mixed oil/ water flow  
 353 and complete gas entrainment to the slug

354 **3.2 Distributed pressure drop**

355 As stated earlier, the first objective of current research is to collect experimental data  
 356 related to flows of viscous oil-water-gas. Thus, more than 200 tests were performed  
 357 to measure three-phase pressure drop. Due to time constraints, the same  
 358 measurement were repeated up to 5 times and the deviations resulted never higher  
 359 than the measurement accuracy (i.e.,  $\pm 1.5\%$  of the pressure transducer full scale).

360 Fig. 9 depicts the results of pressure gradients plotted against  $\epsilon_{Lg}$ , with superficial  
 361 gas velocity as a parameter. Regular trends are observed, that is, for fixed amount of  
 362 gas, increasing liquid superficial velocity (reducing gas to liquid ratio) would result  
 363 in increasing of pressure gradient. At low gas values, this increase in pressure drop is  
 364 more dramatic because we observed a transition from slug to plug flow regimes.



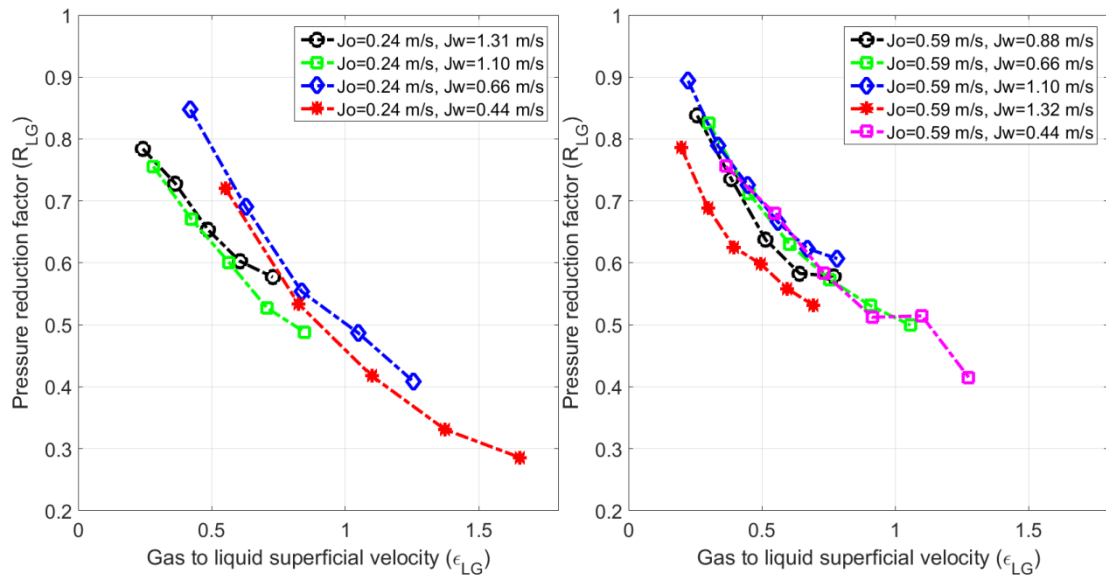
365  
 366 **Fig. 9.** Measured pressure drop ( $\frac{\Delta P}{L}$ ) versus the ratio of gas to liquid superficial  
 367 velocities ( $\epsilon_{Lg}$ )

368 Therefore, the pipe cross-sectional area has a wider contact with liquid, resulting in  
 369 increasing frictional shear stresses. Analysis of pressure drop supports the  
 370 assumption that liquid phases can be treated as equivalent liquid because no  
 371 scattered data of pressure drop observed for fixed gas flow rate.

372 As investigated by other researchers (see e.g. Oliemans and Ooms, 1986, Colombo  
 373 et al., 2015), oil-water core-annular flow regime is of practical interest for heavy oil  
 374 transportation because of high stability and ability to reduce pressure drop. However,

375 as pressure is reduced the amount of dissolved gas in oil is released, so the presence  
 376 of gas to liquid-liquid flow needs to be evaluated. It would be suitable to calculate  
 377 pressure reduction factor for three phase flow to evaluate the influence of air  
 378 addition to liquid-liquid flow, as performed by Bannwart et al. (2004). Fig. 10  
 379 depicts the results of pressure reduction factor versus the ratio of gas to liquid  
 380 superficial velocity ( $\epsilon_{LG}$ ). Two different superficial oil velocities are investigated  
 381 ( $J_o=0.24 \text{ m}\cdot\text{s}^{-1}$  and  $J_o=0.59 \text{ m}\cdot\text{s}^{-1}$ ). Pressure reduction factor has a physical meaning  
 382 in a sense that if  $R_{LG} < 1$  addition of gas has a positive effect and total frictional  
 383 pressure drop is reduced. These results can be justified, considering the fact that gas  
 384 has much lower viscosity than oil and water. Therefore, the increasing gas flow rate  
 385 would result in reducing wall shear stresses and pressure gradient.

386



387

388 **Fig. 10.** Pressure reduction factor versus the ratio of gas to liquid superficial  
 389 velocity for  $J_o=0.24 \text{ m}\cdot\text{s}^{-1}$  and  $J_o=0.59 \text{ m}\cdot\text{s}^{-1}$

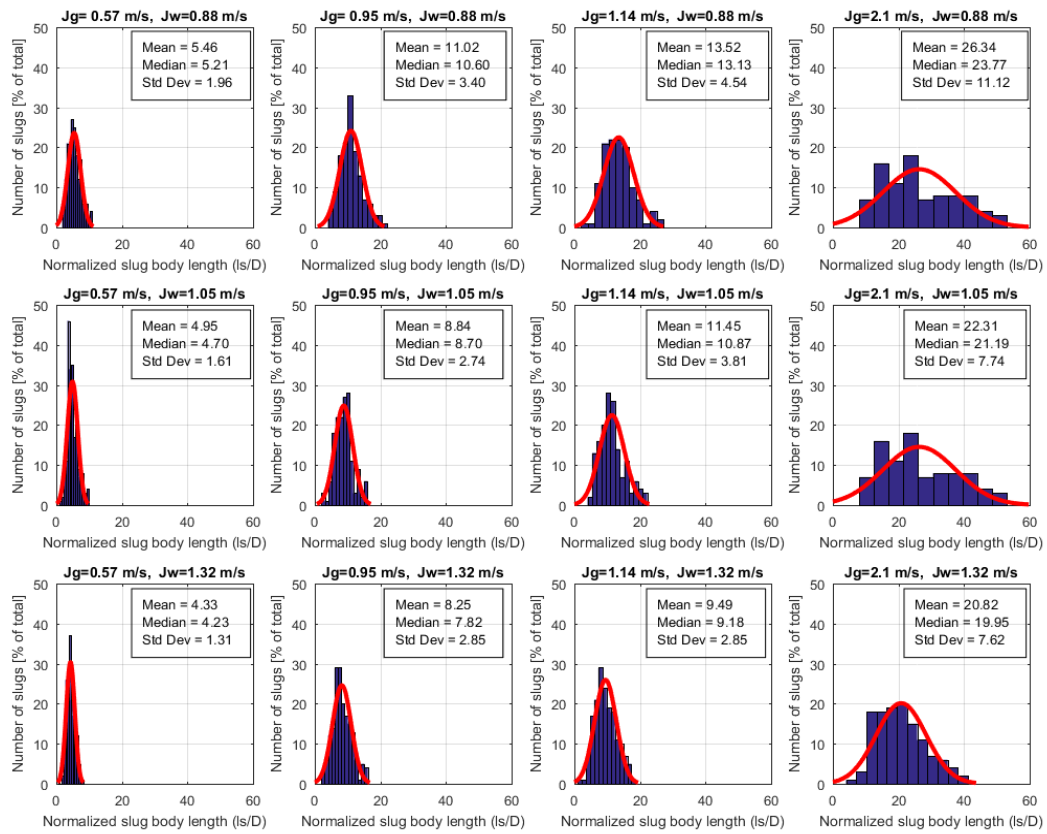
390 Poesio et al. (2009) showed that this phenomenon occurs when flow regime of oil-  
391 water is core-annular. In conditions where transition from core-annular to stratified  
392 flow exists, no regular trend can be observed and repeatability is difficult to be  
393 obtained.

394

### 395 **3.3 Slug body length**

396 Because slug flow regime is a stochastic process, varied slug length can be  
397 discovered along the pipe fluctuated around its average value. So, it is widely  
398 accepted that the log-normal distribution can properly represent the slug body length  
399 as proposed by Losi et al (2016b), Fabre and Line (1992), and shown in Figs. 11-12.  
400 The results of slug body length distribution for two various superficial oil velocities  
401 ( $J_o=0.48 \text{ m}\cdot\text{s}^{-1}$  and  $J_o=0.71 \text{ m}\cdot\text{s}^{-1}$ ) are considered. On abscissa the slug body length  
402 normalized by pipe diameter and on ordinate the number of slugs captured by optical  
403 probe was plotted. In each plot, superficial gas velocity increases from left to right  
404 while superficial water velocity increases from top to bottom. Moreover, mean,  
405 median, and standard deviation values are presented. For fixed oil and water  
406 superficial velocity, as superficial gas velocity rises from  $0.57 \text{ m}\cdot\text{s}^{-1}$  to  $2.1 \text{ m}\cdot\text{s}^{-1}$ , slug  
407 body length increases. The shape of distribution is shifted from highly right-skewed  
408 to normal like one. The number of slugs is considerably reduced due to the longer  
409 elongated bubble. As oil superficial velocity increases at constant water and gas  
410 superficial velocities, shorter slug length with higher frequency was observed.  
411 However, the shape of log-normal distribution remains unchanged. The effect of gas

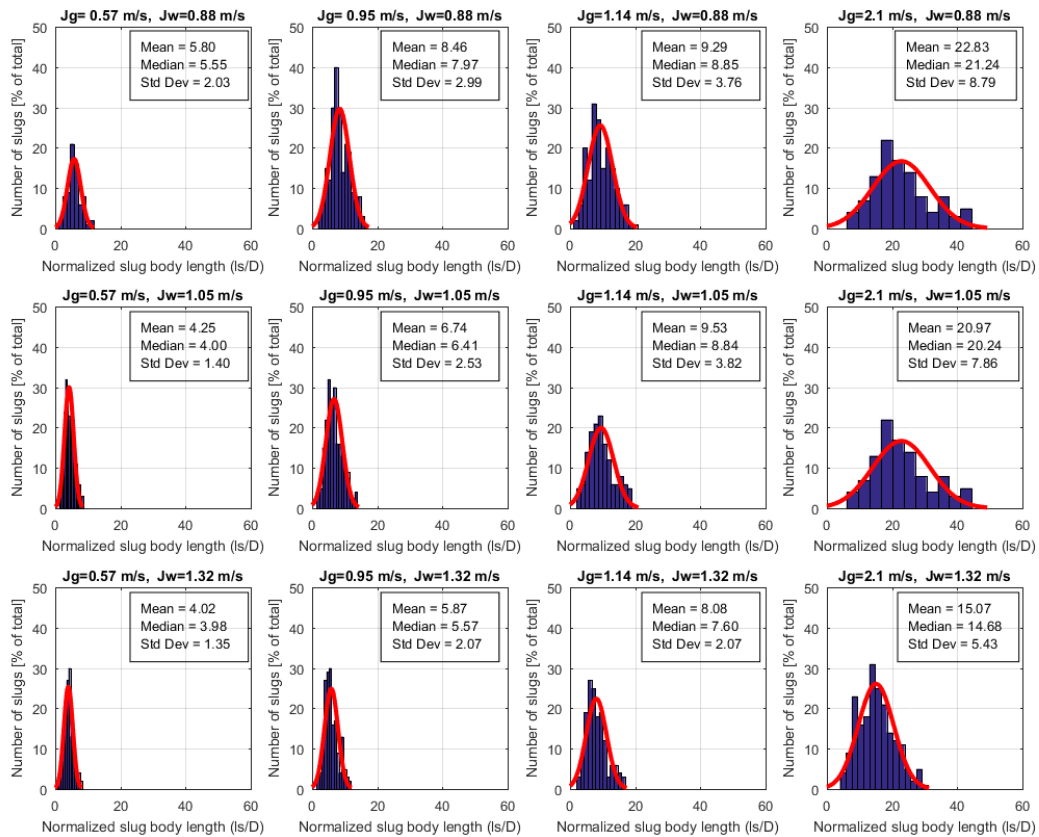
412 superficial velocity is much more dramatic than liquid superficial velocity, probably  
 413 because of pickup rate of slug by bubble (Bubble moving along stratified layer  
 414 pickups liquid at their head), which finally depends on gas superficial velocity.



415

416

**Fig. 11.** Slug body length PDFs for  $J_0 = 0.48$  m/s



417

418

**Fig. 12.** Slug body length PDFs for  $J_o = 0.71$  m/s

419

For two-phase flow of air and water, slug body length ranged between 12-30 D

420

(Dukler and Hubbard, 1975). For two-phase flow with low viscosity of liquid,

421

Barnea and Brauner (1985) proved that slug length is 32D. Al-Safran et al. (2011)

422

measured liquid slug by means of laser and capacitance sensors in high viscosity oil-

423

water. They concluded that average slug length of 10D was a reasonable

424

approximation for high viscosity liquid-gas flow. According to the experimental

425

measurements obtained from optical sensor, the mean slug body length ranged

426

between 3D and 27D. Losi et al. (2016b) experimentally investigated high viscous

427

oil-water flow within a straight duct. They proposed a correlation to compute slug

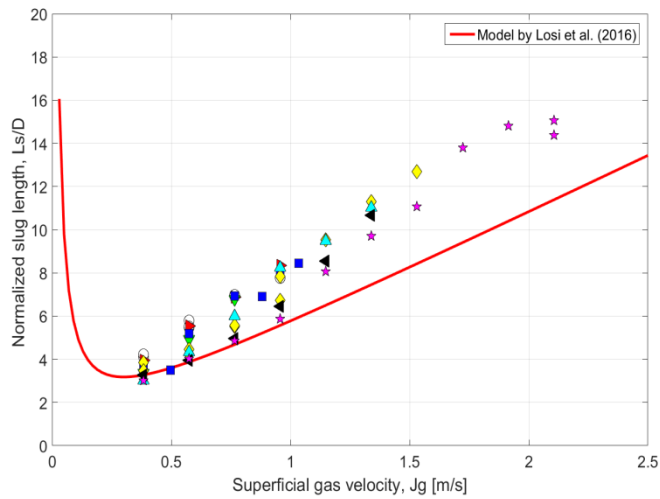
428 body length, considering the effect of both gas superficial velocity and pipe  
429 diameter.

$$430 \quad \frac{L_s}{D} = K \cdot \left( J_g + \frac{J_{go}^2}{J_g} \right) \quad (13)$$

431 Where, K is a constant which depends on liquid properties and  $J_{go}$  is the gas  
432 volumetric flux relating to the shortest slug length. The numerical values of K and  
433  $J_{go}$  were found to be 5.3 and 0.3 from data fitting regression. Slug length data is  
434 compared with the model developed by Losi et al. (2016b) in Fig. 13, while Table 4  
435 shows the comparison between predicted slug length by empirical correlations  
436 (proposed for gas-liquid flow) and experimental counterpart. It is observed in Fig.13  
437 that at low gas superficial velocity, transition from slug to plug and ultimately  
438 dispersed flow regime takes place, leading to infinite length of slug body. It is  
439 evident from Fig. 13 and Table 4 that Barnea and Brauner (1985), and Al-Safran et  
440 al. (2011) models are unable to describe the behaviors of our data, whereas the  
441 approach by Losi et al. (2016b) seems to be consistent, though affected by a rather  
442 large deviation. Average relative error between experimental data and model by Losi  
443 et al. (2016b) is found to be 20.8%, while the maximum relative error is 34%. As  
444 compared to other correlations in Table 4, the lower average relative error and  
445 standard deviation of Losi et al. (2016b) model suggests the strong influence of gas  
446 superficial velocity on slug body length.

447

448



449

450

451

452

453

**Fig. 13.** Slug unit length measured by optical probe versus superficial gas velocity for varied superficial liquid velocity:  $\circ$ : $J_L = 1.36$  m/s,  $\triangleright$ : $J_L = 1.41$  m/s,  $\nabla$ : $J_L = 1.53$  m/s,  $\square$ : $J_L = 1.68$  m/s,  $\diamond$ : $J_L = 1.7$  m/s,  $\triangle$ : $J_L = 1.8$  m/s,  $\triangleleft$ : $J_L = 1.92$  m/s,  $\star$ : $J_L = 2.04$  m/s

454

**Table 4.** Comparison of slug length for different correlations of gas-liquid flow

Correlation	Avg. relative error (%)	Max. relative error (%)	St. deviation (%)
Barnea and Brauner (1985)	454.2	963.1	228.5
Al-Safran et al.(2011)	79.7	232.2	64
Losi et al. (2016b)	20.8	34	10.4

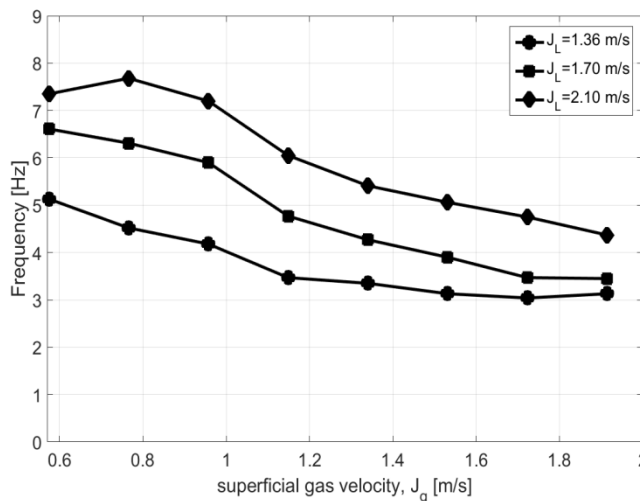
455

456

457

458 **3.4 Slug frequency**

459 The average number of slugs passing through sensors at specified time, inspected by  
460 a stationary observer is defined as slug frequency ( $f_s$ ). The results of slug frequency  
461 as a function of superficial gas velocity are presented in Fig. 14. As superficial gas  
462 velocity increases, decreased slug frequency was observed, showing the presence of  
463 larger elongated bubbles and longer distances between liquid slugs. At fixed gas  
464 flow rate, it can be realized that slug frequency increases and shorter slugs form by  
465 increasing liquid superficial velocity. The agreement between the observed trends of  
466 slug frequency (Fig. 14) with the data of Issa et al. (2007) was satisfactory.



467

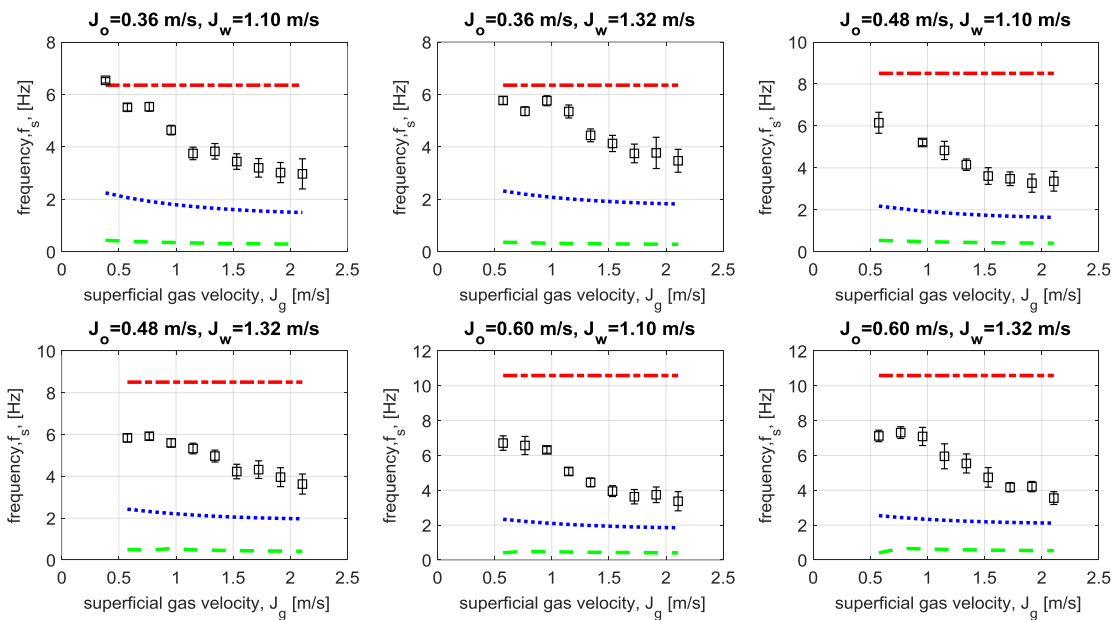
468 **Fig. 14.** Slug frequency versus superficial gas velocity for  $J_L=1.36-2.10$  m·s<sup>-1</sup>

469 In order to check the possibility to broaden the application of gas-liquid flow models  
470 to compute slug frequency for gas-liquid-liquid flow, the experimental data of slug  
471 frequency for different superficial oil and water velocities (ranged within the  
472 intervals of  $0.36 < J_o < 0.60$  m/s and  $1.05 < J_w < 1.32$  m/s) were compared with some of

473 the most used correlations, listed in Table 5. A detailed description of these models  
474 was presented in the study of Hernandez-Perez et al. (2010). Among the models  
475 reported in Table 5, the correlation developed by Gokcal (2010) is based on high  
476 viscosity data and does not consider the influence of superficial gas velocity. The  
477 models developed by Gregory and Scott (1969), Greskovich and Shrier (1972) were  
478 validated for low viscosity liquid-gas flow. It is worth noting that the value of  $J_o$  was  
479 replaced by  $J_L$  for definition of  $\lambda_L=J_o/J_t$  in the latter, to account for the effect of  
480 superficial water velocity. The results of comparisons between predicted values by  
481 the correlations and experimental counterpart are depicted in Fig. 15. The error bars  
482 are also presented, showing standard deviation of each slug frequency (which  
483 implies slug velocity and length) around its average value. As can be seen, all the  
484 models were not capable of describing the behavior of viscous oil-water-gas flow  
485 (see Table 6 for statistical analyses of the model's performance).

486 **Table 5.** Slug frequency correlations for gas-liquid flows from literature

Reference	Correlation	Additional information
Gregory and Scott (1969)	$f_s = 0.0226 \left[ \frac{J_o}{gD} \left( \frac{19.75}{J_t} + J_t \right) \right]^{1.2}$	g:gravitational acceleration D:pipe diameter
Greskovich and Shrier (1972)	$f_s = 0.0226 \left[ \lambda_L \left( \frac{2.02}{D} + Fr_m^2 \right) \right]^{1.2}$	$\lambda_L = J_o/J_t$ $Fr_m = J_t/\sqrt{gD}$
Gokcal et al. (2010)	$f_s = 2.623 \frac{1}{N_f^{0.612}} \frac{J_o}{D}$	$N_f = D^{3/2} \sqrt{\rho_o \Delta \rho g} / \mu_o$



489

490 **Fig. 15.** Comparison between predicted and measured slug frequency. Experimental data is  
 491 shown by square symbol while dashed green line, dotted blue line, and dash-dot red line  
 492 represents the prediction by the models of Gregory-Scott (1969), Greskovich-Shrier (1972), and  
 493 Gokcal et al. (2010), respectively.

494 **Table 6** Frequency relative errors for some gas- liquid prediction correlations

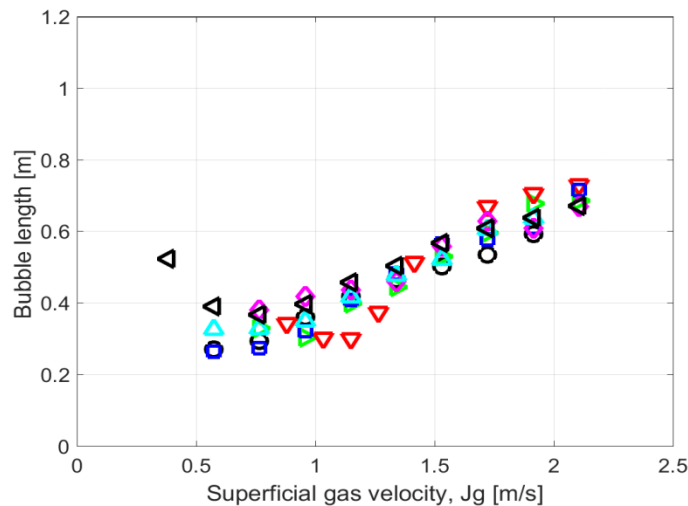
Correlation	Avg. relative error (%)	Max. relative error (%)	St. deviation (%)
Gregory and Scott (1969)	-90.6	-85.0	2.1
Greskovich and Shrier (1972)	-56.2	-40.4	6.6
Gokcal et al. (2010)	87.1	214.2	52.8

495

496

497 **3.5 Bubble and slug unit length**

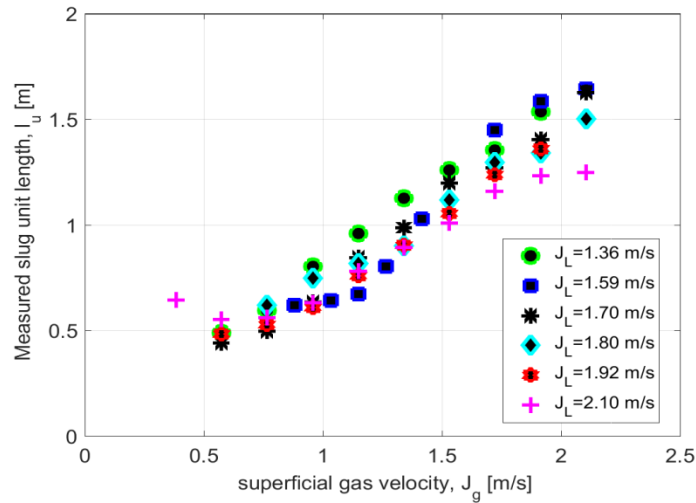
498 In this section, the results of bubble and slug unit length, measured by optical  
499 sensors are presented. Fig. 16 illustrates elongated bubble length as a function of  
500 superficial gas velocity for varied superficial liquid velocities. Not surprisingly,  
501 increases in gas flow rates would result in longer bubbles. The results regarding ~~to~~  
502 slug unit measurements by optical probe versus gas superficial velocity is shown in  
503 Fig. 17. Liquid volumetric flux is considered as a parameter. In Figs. 16 and 17,  
504 different symbols denote various superficial liquid velocities. Apart from liquid  
505 superficial velocity, a regular trend is observed, suggesting considerable effect of  
506 superficial gas velocity on total slug unit length.



507  
508 **Fig. 16.** Measured bubble length by optical probe versus superficial gas velocity  
509 for fixed liquid velocity;  $\circ$ : $J_L = 1.36$  m/s,  $\diamond$ : $J_L = 1.48$  m/s,  $\Delta$ : $J_L = 1.59$  m/s,  
510  $\nabla$ : $J_L = 1.7$  m/s,  $\triangleright$ : $J_L = 1.80$  m/s,  $\square$ : $J_L = 1.92$  m/s,  $\triangleleft$ : $J_L = 2.03$  m/s

511

512



513

514 **Fig. 17.** Measured slug unit length by optical probe versus superficial gas  
515 velocity;  $\circ$ : $J_L = 1.36$  m/s,  $\square$ : $J_L = 1.59$  m/s,  $*$ : $J_L = 1.70$  m/s,  $\diamond$ : $J_L = 1.80$  m/s,  
516  $\star$ : $J_L = 1.92$  m/s,  $+$ : $J_L = 2.10$  m/s

517 As can be seen from Fig. 17, it is possible to justify the behavior of slug unit length based on  
518 the physical mechanism: if the gas velocity is decreased, the structural form of slug flow regime  
519 changes into plug flow and finally followed by dispersed regime. Therefore, as a result of  
520 liquid entrainment into gas bubble, a minimum total slug length is reached. Conversely, when  
521 gas velocity is increased, the total slug unit length increases, following an exponential trend,  
522 as depicted later in Fig. 19.

### 523 3.6 Bubble translational velocity

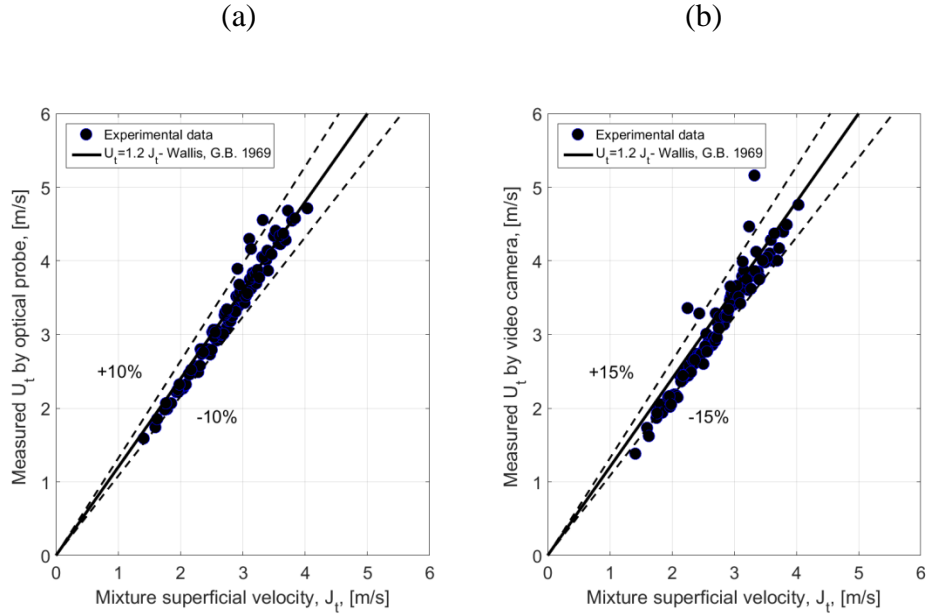
524 Understanding the bubble translational velocity is crucially important because  
525 almost all mechanistic models require the information of this parameter. Bubble  
526 translational velocity has been measured by means of cross-correlation technique,

527 using optical sensor and video camera. It is customary to correlate bubble  
528 translational velocity to mixture superficial velocity. Fig. 18 a-b shows the results of  
529 bubble translational velocity, measured by optical probe and video camera,  
530 respectively. A linear dependency of bubble translational velocity on mixture  
531 superficial velocity is marked for both cases. Larger dispersion of data is observed  
532 for measurement of bubble translational velocity using video camera, probably due  
533 to the lower sampling frequency of video as compared to optical sensor. As first  
534 represented by Nicklin (1962), the experimental data are fitted with the regression  
535 line of  $U_t=C_1 \cdot J_t+C_0$ , where slope ( $C_1$ ) and intercept ( $C_0$ ) of line denotes the  
536 distribution parameter and drift velocity (explained by Fabre and Line (1992) as a  
537 gas bubble velocity moving through stagnant liquid), respectively. Hence, the values  
538 of  $C_0$  becomes 1.2 and 2.0 for fully developed turbulent and laminar flow,  
539 respectively (see, e.g. Foletti et al, 2011).

540 As can be observed from Fig. 18 (a-b), data are well fitted to the correlation of  
541 Wallis (1969) with  $C_0=1.2$  and  $C_1=0$ . The values of drift velocity are in agreement  
542 with other experimental investigations, Farsetti et al. (2014), Losi and Poesio (2016).  
543 The latter evaluated the influence of oil viscosity on drift velocity of a gas bubble  
544 moving in liquids for different axial positions in both horizontal and inclined pipes.  
545 They concluded that drift velocity for viscous oil-gas flow ( $\mu_o=0.804 Pa \cdot s$ ) is ranged  
546 between  $0.0025-0.0065 m \cdot s^{-1}$  for different axial positions in a horizontal pipe, which  
547 can be approximated equal to zero. Although the literature survey immensely suffers  
548 from the lack of experimental data and theoretical modeling to compute translation  
549 bubble velocity for viscous oil-water-air flow, the above analysis showed that

550 application of drift-flux model (which is originally developed for gas-liquid flow)  
551 for three phase flow of viscous oil-water-air leads to a reasonable approximation.

552



553

554

555

556

557

558

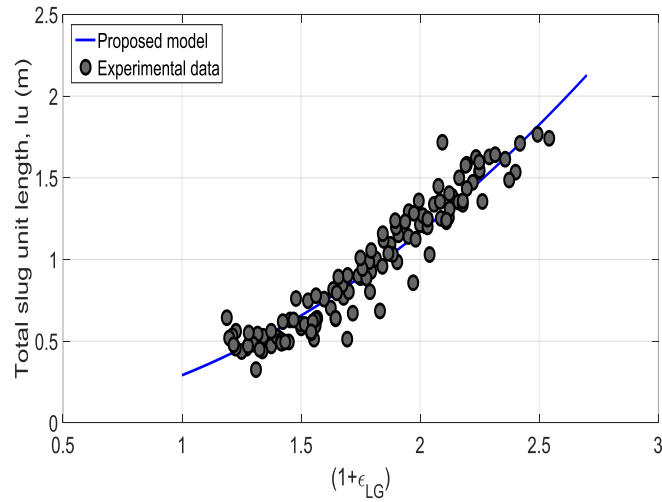
559 **Fig. 18.** Measured bubble translational velocity ( $U_t$ ) versus mixture superficial  
560 velocity ( $J_t$ ) by means of cross-correlation technique using (a) optical sensor, (b)  
561 video camera

562 **3.7 Model development for slug unit length**

563 An attempt was made to correlate the slug unit length to the input flow variables and pipe  
564 diameter. It is worth noting that as the collected data in the present study has a constant surface  
565 tension and viscosity, only inertia forces and pipe diameters are included in the modeling of  
566 total slug unit length. The slug unit length measured by optical probe is plotted against  
567 dimensionless parameter  $(1+\varepsilon_{LG})$  in Fig. 19 to evaluate the influence of liquid and gas  
568 volumetric fluxes on slug unit length. At fixed liquid superficial velocity, increases gas flow  
569 rate causes increasing in slug unit length. All data collapse on a common line, so it is  
570 customary to express slug unit length normalized by pipe diameter with a power law  
571 functional form as function of operating conditions, that is:

$$572 \quad \frac{l_u}{D} = C \cdot (1 + \varepsilon_{LG})^n \quad (14)$$

573 From experimental measurements of total unit length measured by optical sensor, coefficients  
574 C and n are found to be 7.3 and 2, respectively. Equation 14 is valid for  $0.36 < J_o < 0.71 \text{ m}\cdot\text{s}^{-1}$ ,  
575  $0.44 < J_w < 1.32 \text{ m}\cdot\text{s}^{-1}$ , and  $0.22 < J_g < 2.10 \text{ m}\cdot\text{s}^{-1}$ , internal diameter of 40 mm, and oil viscosity of  
576  $0.838 \text{ Pa}\cdot\text{s}$ . Estimation above and beyond this range has to be done by caution as it might  
577 produce inadequate results. The model presented here has to be considered as an operative tool  
578 to compute the total slug unit length; however, it does not aim to describe the physical  
579 mechanism behind such a complex flow. Table 7 lists predicted slug unit cell from proposed  
580 model and experimental data (with respective measured bubble and slug body lengths) from  
581 current study. Those data are provided that the associated flow regimes are available.



583 **Fig. 19.** Experimental total slug unit length measured by optical probe as a function of  
 584 dimensionless parameter  $(\frac{J_t}{J_L})$ .

585 **Table 7.** Comparison of predicted slug unit cell and experimental data

$J_o$ ( $m \cdot s^{-1}$ )	$J_w$ ( $m \cdot s^{-1}$ )	$J_g$ ( $m \cdot s^{-1}$ )	$L_b$ (Measured) (m)	$L_s$ (Measured) (m)	$L_u$ (Measured) (m)	$L_u$ (Prediction) (m)	Relative error (%)	Flow regime
0.36	1.05	0.57	0.19	0.29	0.49	0.57	17.5	Slug-CA
		0.76	0.26	0.30	0.57	0.69	21.4	Slug-FM-PGE
		0.95	0.37	0.34	0.71	0.82	15.1	Slug-FM-PGE
		1.14	0.52	0.43	0.9	0.96	0.15	Slug-FM-PGE
		1.91	0.94	0.55	1.50	1.61	7.8	Slug-FM-CGE
		2.1	1.01	0.59	1.60	1.80	1.6	Slug-FM-CGE
1.32		0.57	0.16	0.32	0.48	0.52	7.4	Slug-CA
		0.76	0.24	0.36	0.60	0.61	2.0	Slug-FM-CGE
		0.95	0.28	0.32	0.61	0.71	17.4	Slug-FM-CGE

		1.14	0.39	0.38	0.78	0.82	5.6	Slug-FM-CGE
		2.1	0.90	0.61	1.52	1.48	-2.8	Slug-FM-CGE
0.71	0.66	0.38	0.14	0.29	0.43	0.47	9.3	Slug-CA
		0.57	0.20	0.29	0.50	0.58	17.1	Slug-CA
	1.32	0.57	0.11	0.35	0.46	0.48	4.2	Slug-FM-CGE
		0.76	0.14	0.32	0.47	0.55	17.7	Slug-FM-CGE
		0.95	0.18	0.35	0.54	0.63	15.8	Slug-FM-CGE
		1.14	0.27	0.42	0.70	0.71	1.9	Slug-FM-CGE
		2.10	0.58	0.61	1.20	1.21	0.69	Slug-FM-CGE

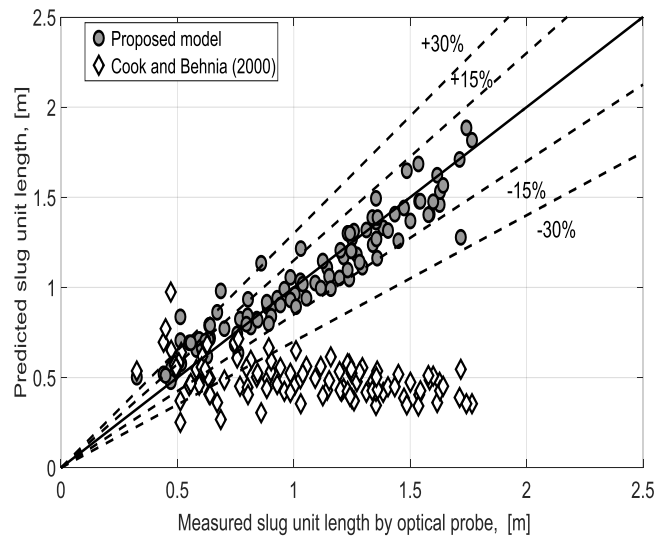
586

587 Due to the lack of experimental data regarding total slug unit for three phase flow of viscous  
588 oil-water-air in the literature survey, the proposed model is only compared with the correlation  
589 developed by Cook and Behnia (2000b). They presented their model for water-air flows, taking  
590 into account bubble length ( $L_b$ ), superficial gas velocity, and liquid holdup in slug body region.

$$591 \quad l_u = \frac{L_b[(1-H_{lf}) \cdot U_t - J_g]}{J_g} \quad (15)$$

592 Where  $H_{lf}$  is the mean liquid holdup in film section. They concluded that the  
593 liquid holdup at bubble head ( $H_{lfe} \sim \frac{U_t - J_t}{U_t}$ ) is different from mean value and  
594 suggested that  $H_{lf}$  can be calculated as  $H_{lf} \sim 1.4 H_{lfe}$ . To make use of equation 15,  
595 information of bubble length is required, which can be obtained from experimental  
596 data. Fig. 20 illustrates the parity plot of predicted slug unit length against  
597 measured slug units using 106 data points. As it is evident, the total slug unit

598 length predicted by proposed model is consistent with experimental data (87% of  
599 all data fall within  $\pm 20\%$  relative error), with the mean absolute relative error of  
600 10.7%. However, The model by Cook and Behnia (2000b) shows a strong under-  
601 prediction, suggesting inability of gas-liquid flow models to predict the slug unit  
602 length (the effect of the third phase (oil) is not considered for model development).



603

604 **Fig. 20.** Parity plot of comparison between experimental data and predicted slug unit  
605 length; dashed lines represent  $\pm 15\%$  and  $\pm 30\%$  deviation from bisector

#### 606 4. Conclusion

607 In this paper, we experimentally studied and analyzed the results of three-phase  
608 flow of viscous oil-water-gas in horizontal pipe. A large number of pressure drop  
609 data set is presented. Due to limitation on operating conditions, only slug flow  
610 regime was considered with oil viscosity of 0.83 Pa.s.

611 Slug body, elongated bubble and total slug unit lengths are experimentally  
612 measured by optical probe. Statistical analysis of slug body length was performed,

613 enabling us to characterize slug flow based on probability density function (PDFs).  
614 It was found that superficial gas velocity had a profound effect on slug body and  
615 bubble length, that is, the higher gas superficial velocity, the longer slug body and  
616 bubble length was observed. A new correlation for slug unit length is developed  
617 based on experimental data obtained by optical probe for three phase flow of  
618 viscous oil-water-gas in horizontal pipe. A good agreement was observed between  
619 predicted slug unit length and measurements, considering almost all data fall into  
620  $\pm 20$  deviation from actual values. Translation velocity of slug unit is measured by  
621 both optical probe and image processing techniques. A modified version of drift-  
622 flux model developed by Nicklin (1962) used to validate experimental data of  
623 translational bubble velocity, showing a good agreement with actual data.

## 624 **Acknowledgement**

625 The authors would like to acknowledge Professor Pietro Poesio for allowing the use  
626 of the optical probe developed at “Laboratorio di Fisica Tecnica Industriale” of  
627 University of Brescia.

## 628 **References**

- 629
- 630 Arnone, D. (2017). Experimental study of two-phase flow air-oil in water emulsion in horizontal  
631 pipes. PhD Thesis. PhD Programme in Mechanical and Industrial Engineering, University  
632 of Brescia (Italy).
- 633 Acikgoz, M., Franca, F., Lahey JR, R.T. (1992). An experimental study of three-phase flow  
634 regimes. *International Journal of Multiphase Flow*, 18, 327-336.
- 635 Al-Safran, E., Gokcal, B., Sarica. C. (2011). High viscosity liquid effect on two-phase slug length  
636 in horizontal pipes. Presented at the 15th International Conference on Multiphase  
637 Production technology. Cannes, France, Jun 15-17.

638 Al-Safran, E., Kora, C., Sarica C. (2015). Prediction of slug liquid holdup in high viscosity liquid  
639 and gas two-phase flow in horizontal pipes. *Petroleum Science and Engineering*, 133, 566-  
640 575.

641 Bannwart, A.C., Rodriguez, O.M.H., Trevisan, F.E. (2009). Experimental investigation on liquid-  
642 liquid-gas flow: Flow patterns and pressure gradient. *Petroleum Science and Engineering*,  
643 65, 1-13.

644 Bannwart, A.C., Rodriguez, O.M.H., Trevisan, F.E., Vieira, F.F., De Carvalho, C.H.M. (2004).  
645 Flow patterns and pressure gradients in horizontal upward inclined and vertical heavy oil-  
646 water-gas flows: experimental investigation and full-scale experiments. 3rd International  
647 Symposium on Two-Phase Flow Modelling and Experimentation. Pisa, Italy.

648 Barnea, D., Brauner, N. (1985). Holdup of the liquid slug in two phase intermittent flow.  
649 *International Journal of Multiphase Flow*, 11, 43-49.

650 Beggs, H.D., Brill, J.P. (1973). A study of two-phase flow in inclined pipes. *Journal of Petroleum*  
651 *Technology. Transaction*, 607-617.

652 Colombo, L.P.M., Guilizzoni, M., Sotgia, G.M., Marzorati, D. (2015). Influence of sudden  
653 contractions on in situ volume fractions for oil-water flows in horizontal pipes. *Journal of*  
654 *Heat and Fluid Flow*, 53, 91-97.

655 Cook, M., Behnia, M. (2000b). Slug length prediction in near horizontal gas-liquid intermittent  
656 flow. *Chemical Engineering Science*, 55, 2009-2018.

657 Dukler, A.E., Hubbard, M.G. (1975). A model for gas-liquid slug flow in horizontal and near  
658 horizontal tubes. *Industrial and Engineering Chemistry*, 14.

659 Fabre, J., Line, A. (1992). Modeling of two-phase slug flow. *Fluid Mechanics*, 24, 21-46.

660 Farsetti, S., Farise, S., Poesio, P. (2014). Experimental investigation of high viscosity oil-air  
661 intermittent flow. *Experimental Thermal and Fluid Science*, 57, 285-292.

662 Foletti, C., Farise, S., Grassi, B., Strazza, D, Poesio, P. (2011). Experimental investigation on two-  
663 phase air/high-viscosity-oil flow in a horizontal pipe. *Chemical Engineering Science*, 66,  
664 5968-5975.

665 Gao, Z., Dang, W., Mu, C., Yang, Y., Li, S., Grebogi, C. (2018). A novel multiplex network-based  
666 sensor information fusion model and its application to industrial multiphase flow system.  
667 *IEEE Transactions on industrial informatics*, 14(9), 3982-3988.

668 Gao, Z., Li, S., Dang, W., Yang, Y. (2017). Wavelet multiresolution complex network for  
669 analyzing multivariate nonlinear time series. *International Journal of Bifurcation and*  
670 *Chaos*, 27, 1750123.

671 Gao, Z., Yang, Y., Zhai, L., Jin, N., Chen, G. (2016). A four-sector conductance method for  
672 measuring and characterizing low-velocity oil-water two-phase flows. *IEEE Transactions*  
673 *on Instrumentation and Measurement*, 65(7), 1690-1697.

674 Gokcal, B., Al-Sarkhi, A.S., Sarica, C., Al-Safran, E.M. (2010). Prediction of slug frequency for  
675 high-viscosity oils in horizontal pipes. *Society of Petroleum Engineers Projects, Facilities*  
676 *& Construction*, 5, 136-144.

677 Gregory, G.A., Scott, D.S. (1969). Correlation of liquid slug velocity and frequency in horizontal  
678 cocurrent gas-liquid slug flow. *American Institute of Chemical Engineers*, 26, 933-935.

679 Greshovich, E.J., Shrier, A.L. (1972). Slug frequency in horizontal gas liquid slug flow.  
680 *Industrial & Engineering Chemistry Process Design and Development*, 11, 317-318.

681 Hall, A. (1992). Multiphase flow of oil, water and gas in horizontal pipes, PhD thesis. Imperial  
682 College, London, UK.

683 Hernandez-Perez, V., Azzopardi, B.J., Kaji, R., Da Silva, M.J., Beyer, M., Hampel, H. (2010).  
684 Wisp-like structures in vertical gas-liquid pipe flow revealed by wire mesh sensor studies.  
685 *International Journal of Multiphase Flow*, 36, 910-915.

686 Hewitt, G. (2005). Three-phase gas-liquid-liquid flows in the steady and transient states. *Nuclear*  
687 *Engineering and Design*, 235, 1303-1316.

688 Issa, R.I., Barbeau, S., Hale, C.P., Odozi, U., Hewitt, G.F., Richardson, S.M., Wong, W.L. (2007).  
689 Measurement and prediction of slug characteristics in three-phase flows. 13th International  
690 conference on multiphase production technology. 13-15 June, Edinburgh, UK.

691 Keskin, C., Zhang, H.Q., Sarica, C. (2007). Identification and classification of new three-phase  
692 gas/oil/water flow patterns. Presented at the SPE annual technical conference and  
693 exhibition. Abaheim, California, USA, 11-14 November. SPE-110221-MS.

694 Losi, G., Arnone, D., Correra, S., Poesio, P. (2016b). Modelling and statistical analysis of high  
695 viscosity oil/air slug flow characteristics in a small diameter horizontal pipe. *Chemical*  
696 *Engineering Science*, 148, 190-202.

697 Losi, G., Poesio, P. (2016). An experimental investigation on the effect of viscosity on bubbles  
698 moving in horizontal and slightly inclined pipes. *Experimental Thermal and Fluid Science*,  
699 75, 77-88.

700 Malinowsky, M. (1975). An experimental study of oil-water and air-oil-water flowing mixtures in  
701 horizontal pipes. MS Thesis. The University of Tulsa, US.

702 Nicklin, D. (1962). Two-phase bubble flow. *Chemical Engineering Science*, 17, 693-702.

703 Odozi, U. (2000). Three-phase gas/liquid/liquid slug flow. PhD thesis. Imperial College, London,  
704 UK.

705 Oliemans, R.VA., Ooms, G. (1986). Core-annular flow of oil and water through a pipeline.  
706 *Multiphase Science and Technology*, 2.

707 Pan, L., Jayanti, S., and Hewitt, G.F. (1995). Flow patterns, phase inversion and pressure gradient  
708 in air-oil-water flow in a horizontal pipe. Presented at the 2nd International conference on  
709 multiphase flow. Kyoto, Japan.

710 Poesio, P., Sotgia, G., Strazza, D. (2009b). Experimental investigation of three-phase oil-water-air  
711 flow through a pipeline. *International Journal of Multiphase Flow*, 21, 107-122.

712 Poesio, P., Strazza, D., Sotgia, G. (2009). Very viscous oil/water/air flow through horizontal  
713 pipes: Pressure drop measurement and prediction. *Chemical Engineering Science*, 64,  
714 1136-1142.

715 Shmueli, A., Unander, T.E., Nydal, O.J. (2015). Characteristics of gas/water/viscous oil in  
716 stratified-annular horizontal pipe flows. *Offshore Technology Conference*. Rio de Janeiro,  
717 Brazil.

718 Stapelberg, H.H., Mewes, D. (1994). The pressure loss and slug frequency of liquid-liquid-gas  
719 slug flow in horizontal pipes. *International Journal of Multiphase Flow*, 20, 285-303.

720 Wallis, G.B. (1969). *One-dimensional two-phase flow*. New York: McGraw-Hill.

721 Wang, S., Zhang, H.-Q., Sarica, C., Pereyra, E. (2013). Experimental study of high-viscosity  
722 oil/water/gas three-phase flow in horizontal and upward vertical pipes. *Society of  
723 Petroleum Engineers production and operation*, 28(03), 306-316.

724 Zhang, H-Q., Sarica.C. (2006). Unified Modeling of Gas/Oil/Water Pipe Flow - Basic Approaches  
725 and Preliminary Validation. *Society of Petroleum Engineers*, 1(02), 1-7.

726

727